NANO LETTERS

pubs.acs.org/NanoLett Letter

van der Waals π Josephson Junctions

Kaifei Kang,* Helmuth Berger, Kenji Watanabe, Takashi Taniguchi, László Forró, Jie Shan,* and Kin Fai Mak*

Cite This: *Nano Lett.* 2022, 22, 5510−5515 Read Online

ACCESS | Metrics & More | Article Recommendations | SI Supporting Information

ABSTRACT: Proximity-induced superconductivity in a ferromagnet can induce Cooper pairs with a finite center-of-mass momentum and stabilize Josephson junctions (JJs) with π phase difference in superconductor-ferromagnet-superconductor heterostructures. The emergence of two-dimensional layered superconducting and magnetic materials promises a new platform for realizing π JJs with atomically sharp interfaces. Here we demonstrate a thickness-driven 0-π transition in JJs made of $NbSe_2$ (an Ising superconductor) and $Cr_2Ge_2Te_6$ (a ferromagnetic semiconductor). By systematically increasing the $Cr_2Ge_2Te_6$ weak link thickness, we observe a vanishing supercurrent at a critical thickness of ∼8 nm, followed by a re-entrant supercurrent. Near the critical thickness, we further observe unusual supercurrent interference patterns with vanishing critical current around zero in-plane magnetic field. They signify the formation of 0-π JJs (with both 0 and π regions), likely induced by the nanoscale magnetic domains in $Cr_2Ge_2Te_6$.

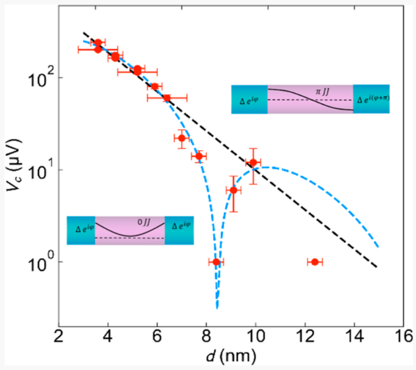

KEYWORDS: *van der Waals Josephson junctions, ferromagnetic Josephson junctions, π Josephson junctions, 0-π transition*

Superconductivity and ferromagnetism are two generally incompatible states of matter and do not coexist in a homogeneous material.[1] At a superconductor-ferromagnet interface, however, Cooper pairs can leak into the ferromagnet and give rise to exotic states, such as the Fulde−Ferrell−Larkin−Ovchinnikov (FFLO) state,[1,2] spin triplet superconductivity,[3] and topological superconductivity.[4−6] In particular, spin-singlet pairing in the ferromagnet with spin-split energy bands would force the Cooper pairs to acquire a center-of-mass momentum; a spatially periodic modulation in the superconducting order parameter known as the FFLO state is developed.[1,2] When the ferromagnet is sandwiched between two superconducting banks to form a Josephson junction (JJ), the superconducting banks can have either a 0 or π phase difference in the ground state depending on the thickness of the ferromagnetic weak link (Figure 1a). Specifically, when the superconducting order parameter at the two interfaces has opposite signs, a π JJ with negative Josephson coupling is stabilized. Although π JJs have been fabricated by evaporation and sputtering of conventional materials,[7,8] the recent discoveries of two-dimensional (2D) layered superconducting[9−12] and magnetic materials[13−15] open a new platform to realize π JJs with atomically uniform thickness and sharp interfaces via van der Waals stacking.[16]

In this study, we report π JJs and a 0-π transition in superconductor-ferromagnet-superconductor (SFS) heterostructures that are made of multilayer $NbSe_2$ (3−10 nm) and $Cr_2Ge_2Te_6$ (CGT for short, 3−13 nm) (Figure 1b). Although such SFS heterostructures have been realized in recent experiments,[17,18] clear evidence of FFLO physics and π JJs has not been demonstrated. Here we resolve this issue through systematic CGT thickness, temperature, and magnetic field dependence studies. Two-dimensional $NbSe_2$ is an Ising superconductor with a thickness-dependent transition temperature around 3−7 K (ref 10). The film thickness is substantially smaller than the out-of-plane penetration depth (∼120 nm[19]) of bulk $NbSe_2$; an in-plane magnetic field thus penetrates the superconductor evenly without flux trapping. The extremely high in-plane upper critical field ∼30−40 T of 2D $NbSe_2$ (ref 10) also renders the superconductor unperturbed by the weak magnetic fields examined in this study. Multilayer CGT is a hole-doped ferromagnetic semiconductor with a band gap around 0.38 eV and a Curie temperature of ∼64 K (ref 20). The in-plane saturation magnetic field is ∼0.5 T (Supporting Information Figure 2), corresponding to relatively weak (out-of-plane) magnetic anisotropy among the known 2D magnetic materials.[15] Moreover, the remanent magnetization is negligible at low temperatures, which is consistent with the formation of nanoscale magnetic domains as revealed by a recent Lorentz transmission electron microscopy (TEM) study.[18]

We examine the Josephson critical current of the junctions as a function of the in-plane magnetic field B and the CGT

Received: April 25, 2022
Revised: June 17, 2022
Published: June 23, 2022

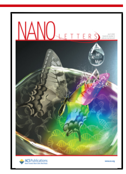

https://doi.org/10.1021/acs.nanolett.2c01640
Nano Lett. 2022, 22, 5510−5515

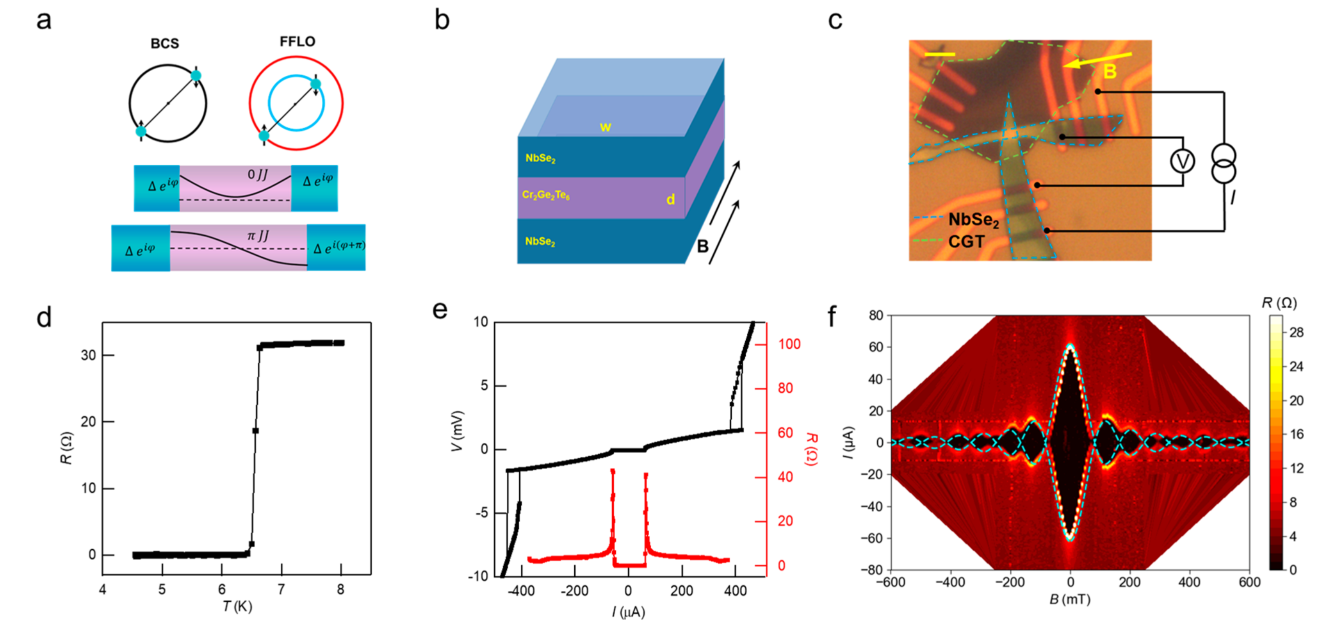

Figure 1. $NbSe_2/Cr_2Ge_2Te_6/NbSe_2$ Josephson junctions. (a) (top) Schematic illustration of spin-singlet Bardeen-Cooper-Schrieffer (BCS) (left) and FFLO Cooper pairs (right). The circles represent the Fermi surface for spin-up and spin-down bands. A finite center-of-mass momentum is developed in the FFLO state. (bottom) 0 and π JJs with superconducting order parameter of the same and opposite sign at the superconductor (blue)-ferromagnet (pink) interfaces, respectively. (b) Schematic of a planar $NbSe_2$/CGT/$NbSe_2$ JJ with barrier thickness d and width w. An in-plane magnetic field B produces a magnetic flux through the cross-sectional area of the JJ. (c) Optical micrograph of JJ01 (3.6 nm thick CGT) together with the measurement circuit. The arrow denotes the magnetic field direction. The dashed lines show the boundary of the flakes. Scale bar is 5 μm. (d) Temperature dependence of the zero-bias differential resistance at zero magnetic field for JJ01. Josephson effect is developed below ~6.5 K. (e) $I-V$ characteristic (black) and the bias-dependent differential resistance (red) at 1.6 K and zero magnetic field. (f) Differential resistance as a function of bias current and magnetic field. Black region denotes zero resistance. The blue dashed line shows the expected Fraunhofer diffraction pattern.

thickness d. The critical current I_c is determined by measuring the differential resistance of the junction $R = \frac{dV}{dI}$ versus a dc bias current I (V denoting the dc voltage across the junction). The junctions are nearly rectangular in shape (Figure 1c). The magnetic field is applied along one of the principal axes in most cases. Because the junction is much smaller than the Josephson penetration depth (see the Supporting Information for estimates), the magnetic flux is uniform in the 2D plane, and the Josephson supercurrent has negligible effects on the flux distribution. Unless otherwise specified, all results are obtained at $T = 1.6$ K, which is substantially below the superconducting transition temperature ($T_c \approx 6-7$ K) of our devices. See the Supporting Information for details on the device fabrication and measurements.

The basic characterization of the JJs is illustrated in Figure 1d−f with device JJ01 as an example (CGT thickness $d \approx 3.6$ nm, total junction thickness 15 nm, and junction width $w \approx 2$ μm). Figure 1d is the temperature dependence of the zero-bias differential resistance at $B = 0$ T. A sharp resistance drop to zero is observed at $T_c \approx 6.5$ K, below which a Josephson supercurrent is established. The current dependences of V and R at 1.6 K are shown in Figure 1e. Zero resistance ($R = 0$ and $V = 0$) is observed below the Josephson critical current $I_c \approx 62$ μA, at which point sharp differential resistance peaks are also observed. The normal state resistance above I_c is $R_n \approx 4$ Ω. The corresponding voltage jump at I_c is $V_c = I_cR_n \approx 240$ μV, which is substantially smaller than the $NbSe_2$ superconducting gap $\Delta \approx 1$ meV (refs 21−24) and is consistent with proximity-induced superconductivity. No hysteresis is detected in the $I-V$ characteristic, showing that the JJ is overdamped.[25] These results suggest a diffusive junction[26] (see below for further discussions). A substantially larger voltage jump that shows hysteresis is observed at a much larger bias current near 400 μA. The voltage jump (>3 mV) exceeds the $NbSe_2$ superconducting gap. It corresponds to the critical current of the superconducting banks and is not related to the Josephson effect investigated in this study.

Figure 1f illustrates the supercurrent interference pattern under an in-plane magnetic field. The boundary separating the finite and zero resistance marks the magnetic-field dependence of the critical current I_c. The critical current is maximum near $B = 0$ T and shows a damped oscillatory dependence on the magnetic field, which is well-captured by a Fraunhofer pattern (dashed line). The oscillation period (70 mT) is consistent with $\Delta B = \frac{\Phi_0}{A_\perp}$, where Φ_0 is the superconducting magnetic flux quantum, and $A_\perp \approx 3 \times 10^{-14}$ m^2 is the cross-sectional area of the junction. The deviation from the ideal Fraunhofer pattern at larger magnetic fields is presumably caused by the internal magnetic field inside the ferromagnetic weak link. These results demonstrate the uniformity of the supercurrent and magnetic flux distributions in the 2D plane of the JJ. No magnetic hysteresis in the interference pattern can be detected for JJs with thin CGTs; this is consistent with negligible remanent magnetization in thin CGTs and negligible flux trappings in the JJs.

We now investigate the CGT thickness dependence of the JJ characteristics. We use the geometry-independent quantity $V_c = I_cR_n$ to characterize the Josephson coupling strength.[8] Figure 2 shows the temperature dependence of V_c for zero-field cooled JJs of several representative CGT thicknesses. The

https://doi.org/10.1021/acs.nanolett.2c01640
Nano Lett. 2022, 22, 5510−5515

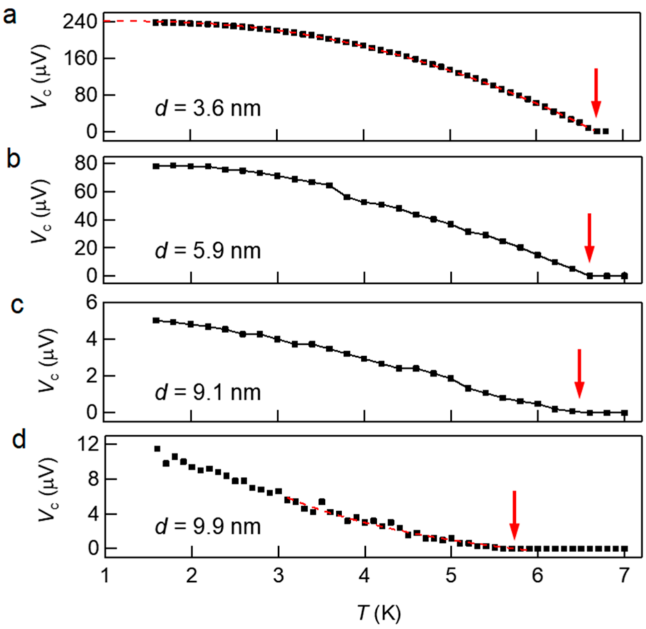

Figure 2. Temperature dependence of V_c. (a−d) Temperature dependence of the critical voltage $V_c = I_cR_n$ for JJs with selected CGT thicknesses of 3.6, 5.9, 9.1, and 9.9 nm. The red dashed line denotes the fit to the Ambegaokar-Baratoff relation in (a) and $V_c \propto \frac{T_c - T}{T}$ near the critical temperature in (d), respectively. Arrows mark the superconducting transition temperature of each device.

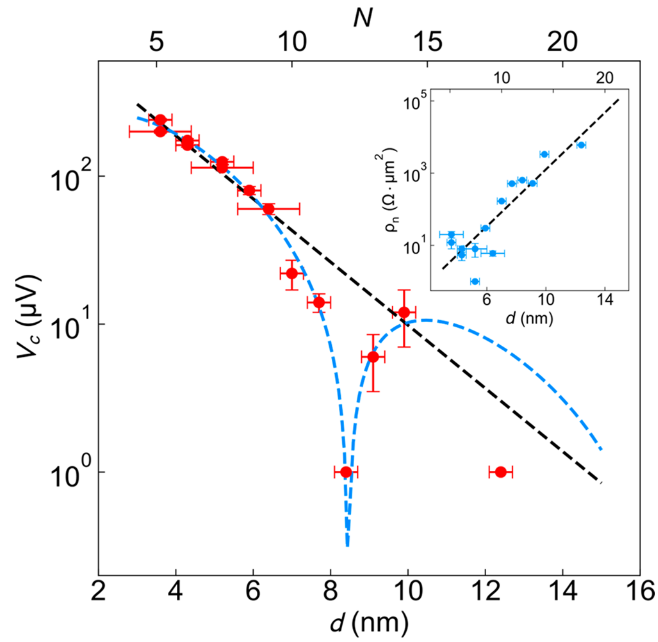

Figure 3. Thickness-driven 0-π transition. Critical voltage V_c as a function of CGT thickness d (bottom axis) or layer number N (top axis). Dashed blue line is the best fit to the data (symbols) with Eqn 1 described in the main text. A 0-π transition is observed at the critical thickness of ∼8.4 nm. The black dashed line illustrates the exponential thickness decay of V_c as a reference. (inset) Thickness dependence of the normal state resistivity of the junctions. Nearly exponential dependence (dashed line) is observed. The vertical error bars of the data are the standard deviations estimated with measurements from different thermal cycles. The thickness error bars are the standard deviations from the atomic force microscopy (AFM) line profiles (Supporting Information Figure 1).

superconducting transition temperature (marked by arrows) varies slightly among different devices because of the slight variations in the $NbSe_2$ thickness. In all cases, V_c ($<\Delta$) becomes finite below T_c and increases monotonically with decreasing temperatures. For JJs with thin CGT barriers (e.g., 3.6 and 5.9 nm), V_c increases linearly near T_c and saturates at low temperatures. The temperature dependence is well-described by the Ambegaokar-Baratoff (AB) relation initially derived for tunnel JJs.[26] For thicker CGT (e.g., 9.9 nm), the temperature dependence substantially deviates from the AB relation; V_c scales approximately as $V_c \propto \frac{T_c - T}{T}$ near T_c.

We approximate the saturated V_c by its value at 1.6 K, the lowest measurement temperature in this study, and show its dependence on the CGT thickness d (bottom axis) and layer number N (top axis) in Figure 3. As CGT thickness increases, V_c first drops quickly, nearly reaches zero at $d_c \approx 8.4$ nm, precedes a revival, and vanishes again at $d \approx 12.3$ nm. (At $d \approx 8.4$ and 12.3 nm, V_c drops below the measurement sensitivity that is limited by the electronic temperature in our experiment; see the Supporting Information.) The observed oscillatory behavior of V_c as a function of the barrier thickness in SFS JJs is a distinctive signature of a thickness-driven 0-π transition in the current-phase relationship induced by FFLO physics.[1,2] In particular, JJs with $d \lesssim 8.2$ nm and $8.2 \lesssim d \lesssim 12.3$ nm have a 0 and π phase difference between the two superconducting electrodes in the ground state, respectively. In contrast, the oscillatory dependence of V_c on temperature is not observed in any junctions (Figure 2). The observed thickness dependence of V_c in Figure 3 can be well-described by a damped oscillatory dependence derived for diffusive SFS junctions with d substantially larger than the coherence lengths[27]

$$V_c = V_{c0} \cdot e^{-d/\xi_{F1}} \cdot \sin\left(\frac{d_c - d}{\xi_{F2}}\right) \quad (1)$$

The best fit (blue dashed line) corresponds to amplitude $V_{c0} \approx 0.94$ mV (which is comparable to the $NbSe_2$ superconducting gap Δ) and coherence lengths $\xi_{F1} \approx 2.5 \pm 0.5$ nm and $\xi_{F2} \approx 2.4 \pm 0.5$ nm for CGT.

In general, the coherence lengths $\xi_{F1,2} \approx \sqrt{\frac{\hbar v_f l}{E_x \mp \pi k_B T}}$ of a ferromagnetic weak link are determined by its scattering mean free path (l), out-of-plane Fermi velocity (v_f), and exchange interaction energy (E_x), with $\hbar$ and k_B denoting the Planck and Boltzmann constants, respectively. Because the CGT Curie temperature (64 K) is much higher than the $NbSe_2$ superconducting transition temperature (∼6 K), the coherence lengths are short below T_c, and the use of Eqn 1 for diffusive SFS junctions is justified. The coherence lengths are also nearly temperature-independent; for the entire range of $0 < T < T_c$, they change by ∼0.1 nm, which is substantially smaller than the CGT interlayer distance of ∼0.7 nm. Temperature-driven 0-π transitions are thus not expected at any fixed CGT thicknesses near d_c. The different temperature dependence of the JJ behavior with different weak link thicknesses (Figure 2) can also be accounted for. For JJs with thin CGT (e.g., 3.6 nm), the junction length (∼d) is comparable to the coherence lengths; the temperature dependence of V_c for a diffusive JJ in this limit is shown to approximately follow the AB relation as in tunnel JJs.[26] As d becomes substantially larger than the

https://doi.org/10.1021/acs.nanolett.2c01640
Nano Lett. 2022, 22, 5510−5515

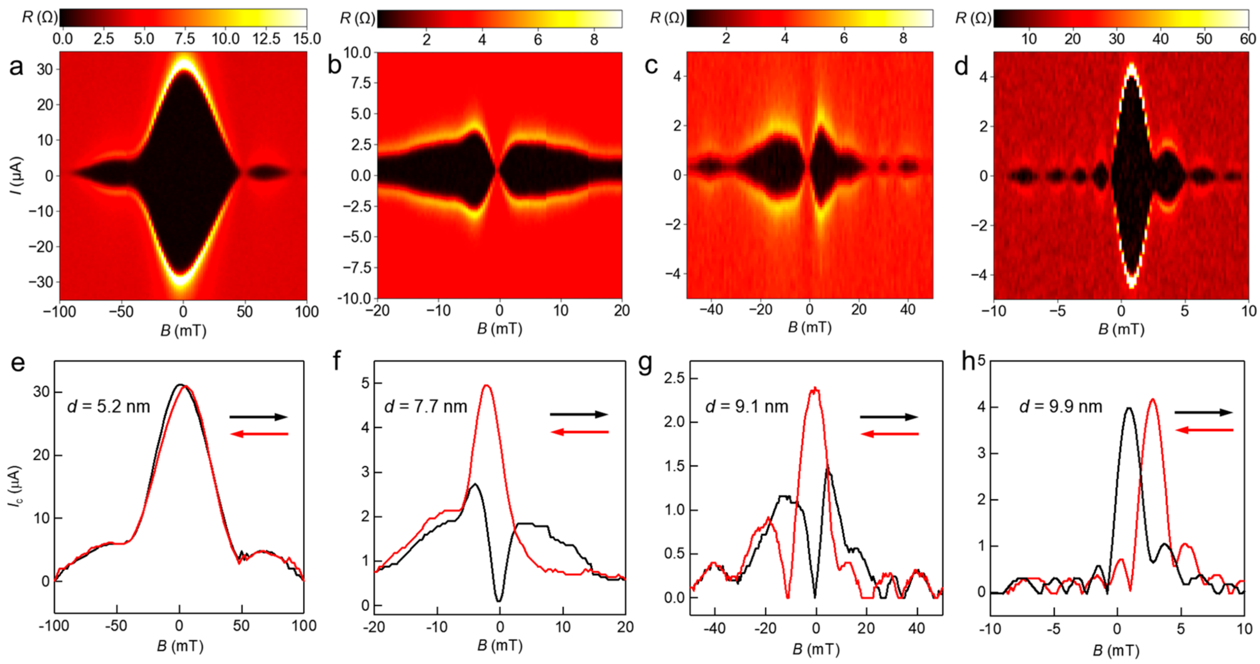

Figure 4. Thickness-dependent supercurrent interference patterns. (a-d) Dependence of the differential resistance on the bias current and magnetic field for JJs with representative CGT thicknesses. The forward field scan is shown. (e–h) Extracted magnetic field dependence of the Josephson critical current for both field scanning directions (denoted by arrows). Fraunhofer-like patterns are observed for d = 5.2 and 9.9 nm; nearly vanishing critical currents at zero magnetic field are observed for d = 7.7 and 9.1 nm for the forward field scan.

coherence lengths (e.g., 9.9 nm), V_c is exponentially suppressed compared to Δ and can be shown to scale as $V_c \propto \frac{T_c - T}{T}$ near T_c (ref 26), as observed in the experiment.

The discussion above treats the CGT weak link as a ferromagnetic conductor with a constant carrier density. The semiconducting nature of CGT and the charge-transfer process at the $NbSe_2$–CGT interfaces are expected to give rise to a nonuniform charge density distribution inside the CGT weak link. Indeed, the junction resistivity ($\rho_n \equiv R_n A$) in the normal state scales with the CGT thickness d exponentially (inset of Figure 3; see the Supporting Information for further discussions), rather than linearly for a constant carrier density (A is the overlap area of the two superconducting banks). The nonuniform charge density distribution also gives rise to a spatially varying Fermi velocity and coherence lengths in the CGT weak link, which can lead to a faster decay of V_c with d compared to the case of a spatially uniform case. Evidence of faster decay at the largest d values is observed in Figure 3 (the JJ with d = 12.3 nm has no measurable critical current).

Finally, we examine in Figure 4 the supercurrent interference patterns in JJs with different CGT thicknesses. The differential resistance contour plots in Figure 4a–d correspond to the forward field scan. The extracted I_c values for both field-scanning directions are shown in Figure 4e–h (arrows denote the field scanning directions). For a CGT thickness away from the critical thickness d_c (i.e., 5.2 and 9.9 nm), a Fraunhofer-like pattern is observed with I_c maximized near B = 0 T. A magnetic hysteresis due to the remanent magnetization and the associated flux lines in CGT is also observed. The hysteresis is more pronounced for the d = 9.9 nm device because it has a much larger cross-sectional area (corresponding to a smaller oscillation period). Remarkably, the interference pattern for CGT thicknesses just one monolayer away from d_c (i.e., 7.7 and 9.1 nm) deviates substantially from the Fraunhofer pattern (Figure 4b,c). The main central lobe is absent, and a vanishing I_c is observed near B = 0 T. For the reversed field scan, an I_c maximum near B = 0 T is restored (Figure 4f,g). These interference patterns are robust for repeated forward and backward field scans within the illustrated magnetic-field range (Supporting Information Figure 3). They are, however, sensitive to magnetic-field cycles to higher fields and to thermal cycles to temperatures above the CGT Curie temperature (Supporting Information Figure 4 and 5). The sensitivity to magnetic-field and thermal cycles is only observed for JJs with $d \approx d_c$.

The emergence of a nearly symmetric double-lobe interference pattern only near $d \approx d_c$ is inconsistent with the stray field effect from the remanent magnetization. The stray field effect would only shift the center of the Fraunhofer pattern away from B = 0 T for all CGT thicknesses. Here the vanishing I_c only near $d \approx d_c$ (for one field scanning direction) indicates the presence of regions of opposite-direction supercurrent within the junction area that nearly cancels each other at B = 0 T. A finite magnetic field destroys the perfect supercurrent cancellation and yields two nearly symmetric critical current lobes around B = 0 T. Such an unusual interference pattern is an experimental signature of a 0-π JJ, a special JJ that possesses spatially separated regions with a 0- and π-phase difference.[28−30] The magnetic hysteresis in the interference patterns and the sensitivity of the patterns to magnetic-field and thermal cycles suggest that the magnetic domain structure of the CGT weak link plays an important role in the formation of 0-π JJs. In particular, a different magnetic domain structure induced by field and thermal cycles destroys the supercurrent cancellation near B = 0 T and the 0-π JJ.

The possibility of stabilizing a 0-π JJ by magnetic domains in a ferromagnetic weak link of uniform thickness is suggested in refs 18 and 31. The magnetic domain walls introduce additional spin-flip scatterings locally and, therefore, spatial

https://doi.org/10.1021/acs.nanolett.2c01640
Nano Lett. 2022, 22, 5510−5515

modulations in the coherence lengths, which in turn modulate the sign of the Josephson coupling across the domain walls for a constant d near d_c and stabilize a 0-π JJ. This mechanism is distinct from what is demonstrated in SFS JJs with varying d within the junction area.[29,30] Such a mechanism is plausible in our devices given the abundance of nanoscale magnetic domains in multilayer CGT.[18] Future studies are required to understand the microscopic origin of 0-π JJs formed for $d \approx d_c$.

In conclusion, we have demonstrated π JJs and a 0-π transition in $NbSe_2$/CGT/$NbSe_2$ SFS heterostructures by systematically varying the CGT thickness. Signatures of 0-π JJs are also observed for thicknesses near the critical thickness d_c. Compared to the JJs in ref 18 that have thin CGT weak links and stronger Josephson couplings, our JJs with thick CGTs are in the diffusive limit; different I−V characteristics and a magnetic response are observed. Further investigations are required to better understand the connection between these two regimes. Moreover, future studies using large band gap ferromagnetic barriers, such as $CrBr_3$ and $CrCl_3$ (refs 15 and 24), can potentially realize tunnel π JJs[32−34] and "quiet" phase qubits.[35−37]

■ ASSOCIATED CONTENT

Supporting Information

The Supporting Information is available free of charge at https://pubs.acs.org/doi/10.1021/acs.nanolett.2c01640.

Device fabrication, electrical measurements, estimate of the Josephson penetration depth, inhomogeneous carrier density in CGT, summary of all JJs, magneto-resistance at the normal state, temperature-dependent supercurrent interference, magnetic history dependent supercurrent interference, dependence of the 0-π interference on thermal cycle, supplementary references (PDF)

■ AUTHOR INFORMATION

Corresponding Authors

Kaifei Kang − *School of Applied and Engineering Physics, Cornell University, Ithaca 14850 New York, United States*; Email: kk726@cornell.edu

Jie Shan − *School of Applied and Engineering Physics, Cornell University, Ithaca 14850 New York, United States; Department of Physics and Kavli Institute at Cornell for Nanoscale Science, Cornell University, Ithaca 14850 New York, United States*; Email: jie.shan@cornell.edu

Kin Fai Mak − *School of Applied and Engineering Physics, Cornell University, Ithaca 14850 New York, United States; Department of Physics and Kavli Institute at Cornell for Nanoscale Science, Cornell University, Ithaca 14850 New York, United States*; orcid.org/0000-0002-5768-199X; Email: kinfai.mak@cornell.edu

Authors

Helmuth Berger − *Institute of Condensed Matter Physics, Ecole Polytechnique Fédérale de Lausanne, Lausanne 1015, Switzerland*

Kenji Watanabe − *National Institute for Materials Science, Tsukuba 305-0044, Japan*; orcid.org/0000-0003-3701-8119

Takashi Taniguchi − *National Institute for Materials Science, Tsukuba 305-0044, Japan*; orcid.org/0000-0002-1467-3105

László Forró − *Institute of Condensed Matter Physics, Ecole Polytechnique Fédérale de Lausanne, Lausanne 1015, Switzerland; Stavropoulos Center for Complex Quantum Matter, Department of Physics, University of Notre Dame, Notre Dame 46556 Indiana, United States*

Complete contact information is available at: https://pubs.acs.org/10.1021/acs.nanolett.2c01640

Notes

The authors declare no competing financial interest.

■ ACKNOWLEDGMENTS

This work was supported by the United States Army Research Office under Grant No. W911NF-17-1-0605 (electrical measurements), the Air Force Office of Scientific Research MURI under Award No. FA9550-18-1-0480 (device fabrication), and the National Science Foundation DMR-1807810 (analysis). It was partially supported by the Cornell Center for Materials Research with funding from the NSF MRSEC program under DMR-1719875 (magnetic characterization). The work made use of the Cornell NanoScale Facility, an NNCI member supported by NSF Grant No. NNCI-2025233. The work in Lausanne was supported by the Swiss National Science Foundation. Growth of the hBN crystals was supported by the Elemental Strategy Initiative of MEXT, Japan, and CREST (JPMJCR15F3), JST.

■ REFERENCES

(1) Buzdin, A. I. Proximity effects in superconductor-ferromagnet heterostructures. *Rev. Mod. Phys.* **2005**, *77*, 935−976.

(2) Eschrig, M. Spin-polarized supercurrents for spintronics. *Phys. Today* **2011**, *64*, 43−49.

(3) Linder, J.; Robinson, J. W. A. Superconducting spintronics. *Nat. Phys.* **2015**, *11*, 307−315.

(4) Zhou, B. T.; Yuan, N. F. Q.; Jiang, H.-L.; Law, K. T. Ising superconductivity and Majorana fermions in transition-metal dichalcogenides. *Phys. Rev. B* **2016**, *93*, 180501.

(5) He, W.-Y.; Zhou, B. T.; He, J. J.; Yuan, N. F. Q.; Zhang, T.; Law, K. T.; et al. Magnetic field driven nodal topological superconductivity in monolayer transition metal dichalcogenides. *Commun Phys* **2018**, *1*, 40.

(6) Kezilebieke, S.; et al. Topological superconductivity in a van der Waals heterostructure. *Nature* **2020**, *588*, 424−428.

(7) Ryazanov, V. V.; et al. Coupling of Two Superconductors through a Ferromagnet: Evidence for a π Junction. *Phys. Rev. Lett.* **2001**, *86*, 2427−2430.

(8) Kontos, T.; et al. Josephson Junction through a Thin Ferromagnetic Layer: Negative Coupling. *Phys. Rev. Lett.* **2002**, *89*, 137007.

(9) Lu, J. M.; et al. Evidence for two-dimensional Ising superconductivity in gated MoS2. *Science* **2015**, *350*, 1353−1357.

(10) Xi, X.; et al. Ising pairing in superconducting NbSe2 atomic layers. *Nat. Phys.* **2016**, *12*, 139−143.

(11) Saito, Y.; et al. Superconductivity protected by spin−valley locking in ion-gated MoS2. *Nat. Phys.* **2016**, *12*, 144−149.

(12) Saito, Y.; Nojima, T.; Iwasa, Y. Highly crystalline 2D superconductors. *Nature Reviews Materials* **2017**, *2*, 16094.

(13) Gong, C.; et al. Discovery of intrinsic ferromagnetism in two-dimensional van der Waals crystals. *Nature* **2017**, *546*, 265−269.

(14) Huang, B.; et al. Layer-dependent ferromagnetism in a van der Waals crystal down to the monolayer limit. *Nature* **2017**, *546*, 270−273.

(15) Mak, K. F.; Shan, J.; Ralph, D. C. Probing and controlling magnetic states in 2D layered magnetic materials. *Nature Reviews Physics* **2019**, *1*, 646−661.

(16) Wang, L.; et al. One-Dimensional Electrical Contact to a Two-Dimensional Material. *Science* **2013**, *342*, 614−617.
(17) Ai, L.; et al. Van der Waals ferromagnetic Josephson junctions. *Nat. Commun.* **2021**, *12*, 6580.
(18) Idzuchi, H.; et al. Unconventional supercurrent phase in Ising superconductor Josephson junction with atomically thin magnetic insulator. *Nat. Commun.* **2021**, *12*, 5332.
(19) Fletcher, J. D.; et al. Penetration Depth Study of Superconducting Gap Structure of 2H-NbSe2. *Phys. Rev. Lett.* **2007**, *98*, 057003.
(20) Wang, Z.; et al. Electric-field control of magnetism in a few-layered van der Waals ferromagnetic semiconductor. *Nat. Nanotechnol.* **2018**, *13*, 554−559.
(21) Dvir, T.; et al. Spectroscopy of bulk and few-layer superconducting NbSe2 with van der Waals tunnel junctions. *Nat. Commun.* **2018**, *9*, 598.
(22) Khestanova, E.; et al. Unusual Suppression of the Superconducting Energy Gap and Critical Temperature in Atomically Thin NbSe2. *Nano Lett.* **2018**, *18*, 2623−2629.
(23) Sohn, E.; et al. An unusual continuous paramagnetic-limited superconducting phase transition in 2D NbSe2. *Nat. Mater.* **2018**, *17*, 504−508.
(24) Kang, K.; Jiang, S.; Berger, H.; Watanabe, K.; Taniguchi, T.; Forró, L.; Shan, J.; Mak, K. F. Giant anisotropic magnetoresistance in Ising superconductor-magnetic insulator tunnel junctions*arXiv*, 2101.01327, 2021 DOI: 10.48550/arXiv.2101.01327.
(25) Tinkham, M. *Introduction to Superconductivity;*McGraw-Hill, 1996; pp 205−206.
(26) Likharev, K. K. Superconducting weak links. *Rev. Mod. Phys.* **1979**, *51*, 101−159.
(27) Weides, M.; et al. High quality ferromagnetic 0 and π Josephson tunnel junctions. *Appl. Phys. Lett.* **2006**, *89*, 122511.
(28) Bulaevskii, L. N.; Kuzii, V. V.; Sobyanin, A. A. On possibility of the spontaneous magnetic flux in a Josephson junction containing magnetic impurities. *Solid State Commun.* **1978**, *25*, 1053−1057.
(29) Frolov, S. M.; Van Harlingen, D. J.; Bolginov, V. V.; Oboznov, V. A.; Ryazanov, V. V. Josephson interferometry and Shapiro step measurements of superconductor-ferromagnet-superconductor 0-π junctions. *Phys. Rev. B* **2006**, *74*, 020503.
(30) Weides, M.; et al. 0-π Josephson Tunnel Junctions with Ferromagnetic Barrier. *Phys. Rev. Lett.* **2006**, *97*, 247001.
(31) Crouzy, B.; Tollis, S.; Ivanov, D. A. Josephson current in a superconductor-ferromagnet-superconductor junction with in-plane ferromagnetic domains. *Phys. Rev. B* **2007**, *76*, 134502.
(32) Caruso, R.; et al. Tuning of Magnetic Activity in Spin-Filter Josephson Junctions Towards Spin-Triplet Transport. *Phys. Rev. Lett.* **2019**, *122*, 047002.
(33) Kawabata, S.; Asano, Y.; Tanaka, Y.; Golubov, A. A.; Kashiwaya, S. Josephson π State in a Ferromagnetic Insulator. *Phys. Rev. Lett.* **2010**, *104*, 117002.
(34) Senapati, K.; Blamire, M. G.; Barber, Z. H. Spin-filter Josephson junctions. *Nat. Mater.* **2011**, *10*, 849−852.
(35) Ioffe, L. B.; Geshkenbein, V. B.; Feigel'man, M. V.; Fauchère, A. L.; Blatter, G. Environmentally decoupled sds -wave Josephson junctions for quantum computing. *Nature* **1999**, *398*, 679−681.
(36) Yamashita, T.; Tanikawa, K.; Takahashi, S.; Maekawa, S. Superconducting π Qubit with a Ferromagnetic Josephson Junction. *Phys. Rev. Lett.* **2005**, *95*, 097001.
(37) Feofanov, A. K.; et al. Implementation of superconductor/ferromagnet/ superconductor π-shifters in superconducting digital and quantum circuits. *Nat. Phys.* **2010**, *6*, 593−597.

https://doi.org/10.1021/acs.nanolett.2c01640
Nano Lett. 2022, 22, 5510−5515